Unexpected circular radio objects at high Galactic latitude

Norris, R.P.; Intema, H.T.; Kapińska, A.D.; Koribalski, B.S.; Lenc, E.; Rudnick, L.; ... ; Whiting, M.

Unexpected Circular Radio Objects at High Galactic Latitude

Ray P. Norris[1,2⋆], Huib T. Intema[4,11], Anna D. Kapińska[3], Bärbel S. Koribalski[1,2], Emil Lenc[2], L. Rudnick[6], Rami Alsaberi[1], Craig Anderson[3], G. E. Anderson[4], E. Crawford[1], Roland Crocker[8], Stefan W. Duchesne[4], Miroslav D. Filipović[1], Andrew M. Hopkins[9], Natasha Hurley-Walker[4], Susumu Inoue[7], Kieran Luken[1,2], Peter Macgregor[1], Pero Manojlović[1], Josh Marvil[3], Andrew N. O'Brien[1,2,5], Wasim Raja[2], Devika Shobhana[1], Jordan D. Collier[1,10], Catherine Hale[2], Aidan Hotan[2], David McConnell[2], Vanessa Moss[2], & Matthew Whiting[2]

[1] *Western Sydney University, Locked Bag 1797, Penrith, NSW 2751, Australia*
[2] *CSIRO Astronomy & Space Science, P.O. Box 76, Epping, NSW 1710, Australia*
[3] *National Radio Astronomy Observatory, PO Box 0, Socorro, NM87801, USA*
[4] *International Centre for Radio Astronomy Research, Curtin University, GPO Box U1987, Perth, WA 6845, Australia*
[5] *Center for Gravitation, Cosmology and Astrophysics, Department of Physics, University of Wisconsin-Milwaukee, PO Box 413, Milwaukee, WI 53201, USA*
[6] *University of Minnesota, 100 Church St SE, Minneapolis, MN 55455, USA*
[7] *Riken, 2-1 Hirosawa, Wako, Saitama, 351-0198, Japan*
[8] *Australian National University, Canberra ACT 2600, Australia*
[9] *Australian Astronomical Optics, Macquarie University, 105 Delhi Rd, North Ryde, NSW 2113, Australia*
[10] *The Inter-University Institute for Data Intensive Astronomy (IDIA), Department of Astronomy, University of Cape Town, Private Bag X3, Rondebosch, 7701, South Africa*
[11] *Leiden Observatory, Leiden University, PO Box 9513, NL-2300RA, Leiden, The Netherlands*
⋆ *e-mail: raypnorris@gmail.com*

We have found an unexpected class of astronomical objects which have not previously been reported, in the Evolutionary Map of the Universe Pilot survey, using the Australian Square Kilometre Array Pathfinder telescope. The objects appear in radio images as circular edge-brightened discs about one arcmin diameter, and do not seem to correspond to any known type of object. We speculate that they may represent a spherical shock wave from an extra-galactic transient event, or the outflow, or a remnant, from a radio galaxy viewed end-on.

1 Introduction

Circular features are well-known in radio astronomical images, and usually represent a spherical object such as a supernova remnant, a planetary nebula, a circumstellar shell, or a face-on disc such as a protoplanetary disc or a star-forming galaxy. They may also arise from imaging artefacts around bright sources caused by calibration errors or inadequate deconvolution. Here we report

the discovery of a class of circular feature in radio images that do not seem to correspond to any of these known types of object or artefact, but rather appear to be a new class of astronomical object. For brevity, and lacking an explanation for their origins, we dub these objects "Odd Radio Circles", or ORCs.

These objects were discovered in the Pilot Survey[1] of the Evolutionary Map of the Universe (EMU)[2], which is an all-sky continuum survey using the newly-completed Australian Square Kilometre Array Pathfinder telescope (ASKAP)[3–5]. The EMU Pilot Survey (EMU-PS) used ASKAP to survey a field of about 270 $\deg^2$ to an rms sensitivity of about 30 μJy/beam, with a spatial resolution of about 12 arcsec. Details of the observations and data reduction, and techniques used for data analysis, are given in the Supplementary Information.

Three ORCs (ORCs 1–3) were discovered by visual inspection of the images from the survey. Their rarity, together with their low surface brightness, makes it unlikely that they could have been discovered in previous radio surveys.

We discovered a further ORC (ORC 4) in archival data taken with the Giant MetreWave Radio Telescope (GMRT)[6] in March 2013. In most respects it is very similar to ORCs 1–3, but differs in having a central radio continuum source.

Figure 1 shows the radio and optical images of the ORC 1 (top), ORCs 2 & 3 (middle) and ORC 4 (bottom).

None of the ORCs has obvious optical, infrared, or X-ray counterparts to the diffuse emission, although in two cases there is an optical galaxy near the centre of the radio emission.

The EMU-PS area is covered by Data Release 1 of the Dark Energy Survey (DES)[7] and we use DES data throughout this paper, together with infrared data from the Wide-field Infrared Survey Explorer (WISE)[8], and, for ORC 4, optical data from the Sloan Digital Sky Survey SDSS[9]. Our current ASKAP and GMRT data do not enable the measurement of polarisation or in-band spectral index for such faint diffuse objects.

ORCs 1–2 were subsequently observed at 2.1 GHz with the Australia Telescope Compact Array (ATCA) resulting in the images shown in Figure 2, and also found in previously observed data at 88–154 MHz with the Murchison Widefield Array (MWA). Details of these observations are given in the Supplementary Information.

2 Properties of the ORCs

Detailed data for objects discussed in this section are given in the supplementary information section.

ORC 1: EMU PD J210357.9–620014 This radio source (diameter $\sim$ 80 arcsec) has a near circular, edge-brightened filled morphology with brighter spots around its periphery. Figure 3 shows the radio contours overlaid on the DES 3-color (gri) optical image. There is no optical emission corresponding to the ring. The typical radio brightness over ORC 1 in the ASKAP image is ~ 130 μJy/beam, with an integrated flux density of 5.45 mJy. By comparing our data from all the radio observations, listed in the Supplementary Information, we derive a spectral index of the diffuse emission of -1.27 ± 0.08. Such a steep spectral index may indicate an ageing electron population, as often found in SNRs, cluster haloes, and dying radio galaxies.

On the southern edge of the ring is a bright radio source (labelled "S" in Figure 2) which is associated with a galaxy detected both by WISE (WISE J210257.88–620046.3) [8] and by GALEX (GALEXASC J210257.91–620045.4) [10]. The WISE colours indicate that this is a star-forming galaxy, and possibly a starburst or LIRG (luminous infrared galaxy). Unfortunately no redshift has been measured for this object.

The radio observations listed in Table 2 show that source S has a spectral index of $\sim -1.24 \pm 0.35$, making it more likely to be an active galactic nucleus (AGN) than a star-forming galaxy. The space density of radio sources in the EMU-PS at least as bright as source S is ~ 390 per deg^2, giving a $\sim 15\%$ probability that this is a unrelated source. It is therefore possible that this is an unrelated object, physically unconnected to the diffuse object.

At the centre of the ring is a faint optical object (WISE J210258.15–620014.4), labelled "C" in Figure 2, with no detectable radio emission in any of our observations. The enlarged DES gri-band image in Figure 3 shows that this central object is extended E-W with a total extent of about 6 arcsec, (c.f. the $\sim$ 1 arcsec resolution of DES) and is probably a galaxy.

The WISE colours for the central object (W1–W2 = 0.079, W2–W3 < 2.045) do not enable us to distinguish between

a star-forming galaxy, or a quiescent galaxy, but the optical colours suggest a quiescent galaxy. Unfortunately no redshift has been measured for this object.

At redshifts greater than 1, 6 arcsec corresponds to a diameter of 40–60 kpc, making it unlikely to be a normal star-forming galaxy at high redshift. The local space density of galaxies

(6333 per sq deg at W1<15) mean that there is a 15 percent probability of there being a source brighter than 15 mag within 10 arcsec of the centre. We therefore consider it possible that this is an unrelated object.

One arcmin to the south-east of the radio source is a 16-magnitude galaxy (WISE J210308.23–620055.0) which is very elongated north-south in the optical image, and also appears as an elongated radio source. The WISE colours of this source are that of a spiral, so we consider it likely to be an edge-on spiral galaxy. It appears to be unconnected to the diffuse radio object and will not be discussed further.

ORC 2: EMU PD J205842.8–573658. Like ORC 1, this unusual radio source (diameter $\sim$ 80 arcsec) has a near circular, edge-brightened filled morphology with brighter spots around its periphery. Figure 4 shows the radio contours overlaid on the DES 3-color (gri) optical image.

The typical brightness over the diffuse object is $\sim$ 100–200 μJy/beam, and the integrated flux density over the object (excluding sources A,B, and C) is $\sim$ 5.8 mJy at 944 MHz.

To the north-east of ORC 2 in the ASKAP image is a pair of strong radio components. The ATCA image (Figure 2) shows a flat-spectrum source between them which is not visible on the ASKAP image, but which appears to be the central component of a double-lobed radio source, and which is within $\sim$ 1 arcsec of the nearby optical galaxy labelled "B". However, this optical galaxy appears to be a 2.5 arcsec extended spiral galaxy, at a redshift of 0.35, which seems to be an unlikely host for a double-lobed radio galaxy, so this may be a chance association.

The space density of components in the EMU-PS at least as strong as source B is about 219 per deg^2, so the probability of finding B within 1 arcmin of the ORC is about 19%, and so we consider it possible that this source is an unrelated object.

Within the eastern limb of ORC 2 in the ASKAP image is a compact radio source which is coincident with the galaxy labelled C is Table 4, which appears to be an edge-on galaxy. The space density of components in the EMU-PS at least as strong as source C is about 1000 per deg^2, so the probability of finding B within 1 arcmin of the ORC is about 90%, and so we consider it likely that this source is an unrelated object.

ORC 3: EMU PD J205856.0-573655. Immediately to the east of ORC 2 is a another faint circular patch, which is visible in two independent observations with ASKAP, but is too faint to be seen in ATCA or MWA data. This faint diffuse patch has a typical brightness of $\sim$ 50–80 μJy/beam, and the integrated flux density over the object is $\sim$ 1.6 mJy at 944 MHz. It has a spectral index of ~ -0.50, although this is quite uncertain because it depends on two upper limits and one detection.

ORC 3 appears to be a fainter example of the ORC phenomenon exhibited by ORCs 1 and 2, but it is puzzling that it is so close to ORC 2. Within the EMU-PS, there are 2 very obvious ORCs (ORCs 1 and 2) and about six fainter "candidate ORCs", giving a space density of ~ 0.03 per deg^2. The probability of one of these lying within 2 arcmin is therefore about 10^{-4}. We therefore consider it unlikely that this is a chance association, but instead deduce that ORC 2 and ORC 3 are in some way related.

ORC 4 We discovered ORC 4 in archival observations of the cluster Abell 2142 taken at 325 MHz with the Giant MetreWave Radio Telescope (GMRT)[6] in March 2013. Details of the observation are given in the supplementary information and in [11]. In most respects ORC 4 is very similar to ORCs 1–3, but differs in having a central radio continuum source.

ORC 4 is marginally detected at 150 MHz in TGSS[12] and at 1.4 GHz in NVSS[13], but in both cases the image quality is poor because of poor sensitivity, uv-coverage, and low resolution. The measured total flux densities are given in Table 3.

Combining all aperture flux measurements, we fit a single spectral index α = –0.93 $\pm$ 0.26. [1]

ORC 4 differs from the other ORCs in having a central radio source, labelled "G" in Figure 1, which is listed in the NVSS catalogue [13] as NVSS J155524+272629. It is coincident with a red galaxy seen in both SDSS and Pan-Starrs images, and detected by WISE. The compact source has an unambiguous optical/IR counterpart in SDSS (SDSS J155524.63+272634.3) and WISE (WISEA J155524.65+272633.7) with a photometric redshift of 0.39[14] implying a linear size of the ring of 430 kpc $\times$ 320 kpc.

Summary of ORC properties The four ORCs discussed here are similar in displaying a strong circular symmetry. They are also similar in (a) having a diameter about 1 arcmin, (b) having a steep spectral index $\alpha \sim -1$ (c) being at high Galactic latitude. They differ in that (a) two of them have a central galaxy while two do not, and (b) three of them (ORCs 1, 2 & 4) consist of a partly filled ring while one (ORC 3) seems to be a uniform disc. The radial profiles of the ORCS are shown in Figure 6. ORC 1, ORC 2, and ORC 4 are similar in having a filled but edge-brightened disc, while ORC 3 decreases monotonically from the centre.

There is also the puzzling fact that two of them are very close together, implying that these two ORCs have a common cause.

If the central galaxy in ORC 4 is associated with the ring, then the ring is at a redshift of 0.39 and has a size of 350 $\times$ 280 kpc.

[1]For a source with flux density S at frequency ν, we define spectral index α as $S \propto \nu^{\alpha}$

We estimated proper motion by comparing the positions of ORCs 1 and 2 in the ASKAP (taken in November 2019) and ATCA observations (taken in March 2020). This is difficult because of their diffuse nature and the low SNR of the ATCA observations, but we estimate an upper limit of about 4 arcsec on any spatial shift of the diffuse emission between the two sets of observations, which rules out a solar system object.

3 Discussion

We now consider possible explanations of these objects. For the purposes of this discussion, we assume all four to have a similar cause, although we acknowledge that it is possible that we may have more than one type of object represented in the class of ORCs.

Imaging Artefact Circular artefacts are well-known in radio images, and are often caused by imperfect deconvolution of a strong source, resulting in some fraction of the telescope point-spread-function appearing in the final image. However, ORCs 1 and 2 are clearly imaged with two different telescopes, at different times, with different processing software, and all ORCs have been detected by more than one telescope. We therefore consider artefacts to be a very improbable explanation.

Supernova Remnant The morphology of the ORCs is remarkably similar to some typical supernova remnants (SNRs) [15–19]. We calculate the probability that the ORCs are SNRs as follows. The EMU-PS covers about 270 sq deg of sky at a galactic Latitude of 40°. We therefore model the EMU-PS as a cone of half-angle 9.3° at an angle of 40° (the Galactic latitude) from the mid-plane of a disc 1 kpc thick. The volume of Galaxy being surveyed by EMU-PS is therefore 0.02 kpc^3. Assuming the Galaxy to be a uniform disc of radius 10 kpc and thickness 1 kpc, the fraction of the Galaxy surveyed by EMU-PS is therefore 6×10^{-5}, in which we detect 3 ORCs. If the ORCs are SNR, then this implies the Galaxy contains ∼50,000 SNRs. There are ∼350 confirmed SNRs in the Galaxy [17]. Even if the Galactic population were as high as 1000 SNRs, the probability of finding one of them in EMU-PS, assuming they are uniformly distributed, is 6%, and the probability of finding three is 0.02%. We therefore consider it unlikely that these are SNRs.

Galactic Planetary Nebula Planetary nebulae (PNe) can also appear as diffuse disks of radio emission [20]. The spectral index α of PNe are reported in two surveys [21,22] to be in the range $-1 \leq \alpha \leq +1$. However, both surveys suffer from large uncertainties because of poor frequency coverage. It has aslo been argued [23] that optically thick PNe have a radio spectral index α ∼+2 and optically thin PNe have α ∼–0.1, neither of which is close to the typical spectral index of ORCs of $\alpha \sim$ –1.

However, the strongest argument against PNe as an explanation for ORCs is that only about

3000 PNe are known[24], so following the same argument as for SNRs, the probability of finding three in the EMU-PS is about 0.05%. We therefore consider it unlikely that the ORCs are PNe.

Face-on star-forming galaxy or ring galaxy Ring-shaped star-forming galaxies such as the Cartwheel galaxy are well-known [25], and some nearby, nearly face-on spiral galaxies have star-forming rings, typically detected in the Hα emission line and in radio continuum [26,27]. An example detected by ASKAP is shown in Figure 7. However, in all known cases these ring galaxies and starburst rings are bright at optical wavelengths, which contrasts with the lack of measurable optical emission from the ORCs on a similar scale to the radio emission. If the ORC emission corresponded to the size of a typical disk galaxy ($\sim$10–20 kpc) it would lie at a distance of about 25–50 Mpc ($z \sim 0.01$). The emission from such a large, nearby face-on disk galaxy would be easily detectable in the DES imaging. We therefore do not consider these to be a likely explanation for ORCs.

Lobe from a double-lobed radio galaxy, viewed side-on The ORCs might, in principle, be one lobe of a double-lobed radio galaxy. For example, the radio galaxy Fornax A has two near-circular radio lobes, shown in Figure 8. However, we consider this unlikely for the following reasons:

- The ORCs are strikingly circular, and edge-brightened, unlike the morphology typically seen in double-lobed radio galaxies.
- While ORCs 2 and 3 could conceivably be a double-lobed radio source, there is no corresponding lobe to ORCs 1 or 4.
- For ORCs 2 and 3, there is no sign of a central optical or radio host source between the two lobes. Source C in the limb of ORC 2 could potentially be a host, but it is an edge-on spiral galaxy, which rarely host double-lobed radio sources.
- For ORCs 2 and 3, the brightnesses of the two lobes are quite different, in which case we would also expect morphological differences between the lobes, and yet they have identical sizes and shapes.

Lobe from a double-lobed radio galaxy, viewed end-on If a radio-loud AGN is viewed "down the barrel" of the jet, the end-on radio lobe can appear as a circular object, as seen in some BL Lac sources [28]. If the central radio source were precessing, then the central spot could in principle be a circle, although this has not yet been observed. However, such sources are accompanied by (in the case of a BL Lac source) a bright, blue, unresolved (sub-arcsec) optical counterpart, or (in the case of a radio galaxy) by a quiescent galaxy, and neither of these are seen in ORCs 2 and 3. Furthermore, in such sources, the central radio emission is brighter than the fainter halo.

There is also a problem with the inferred physical sizes. If the ORCs are at redshifts at $z \sim$ 0.4 – 1, which is consistent with faint optical counterparts and with the measured redshift of source

G in ORC 4, then the transverse sizes would be of order of 500 kpc, which is more than an order of magnitude greater than is observed in other radio galaxies.

Another possibility is that a population of radio galaxies with edge-brightened lobes, such as the one in Figure 9, could provide the parent population. This source has a total extent of 150" and a width of 40", with an edge on the southern lobes that is 30-50% brighter than the central regions of the lobe. Such extremely faint sources would be detected more easily when viewed end-on, where they would appear ORC-like. However, such sources would still have a bright central AGN, which is not seen in all ORCs, and the inferred transverse sizes of 100s of kpc appear implausible.

ORC-like structures could also appear from the end-on view of bubbles or tori from buoyantly rising old lobes of radio galaxies in a cluster atmosphere [29,30]. In a later stage of evolution, these could even be re-energized and become visible through collisions with shocks [31] and be responsible for elliptical ring-like radio "relics" produced during cluster mergers [32], if seen edge on. However, these suffer from the problems that (a) such relics do not have the strong circular symmetry of the ORCs, and (b) no cluster is seen associated with most ORCs,

Another possibility is that a radio galaxy can leave behind a blob of plasma, which can then form a vortex ring if it encounters a shock. Although the initial shape of the ring is likely to be irregular, reflecting the irregular intersection cross section, the vortex ring is self-propagating and tends to circularize with time [33,34]. Such a blob/shock encounter was proposed to explain the large ring at the end of NGC 1265 [35]. After the AGN has turned off, the re-energized synchrotron-emitting ring may not show any obvious connection to its parent galaxy.

A bent-tail radio galaxy In a bent-tail radio galaxy, the two jets are bent/curved by their relative motion through the intra-cluster medium. In the case of the source shown in Figure 10, the bending is so severe as to form almost a circle, and its formation would require additional forces or jet variations over and above relative motion. In the case of ORC 1, it could be argued that source S is the host galaxy. However, jets from SF galaxies are rare, and bent ones have not yet been seen. Similar to the ORCs, there is faint central emission between the bent tails, approximately 30% as bright as the tails. However, no bent-tail galaxy, in including the source shown in Figure 10, shows the striking circular symmetry of the ORCs, and so we do not consider this to be a likely cause of the ORCs.

Einstein Ring Gravitational lensing of background sources can produce arcs of emission. If the source, lens, and observer are aligned, then the lensed image can take the form of a so-called Einstein ring. For example, the radio gravitational (compound) lens PKS 1830–211, consists of a $\sim$1 arcsec diameter ring [36]. However, such Einstein rings are rarely more than a few arcsec in diameter. Much larger gravitational lenses are known [37] but the lensed image in such cases is irregular, consisting of a number of sub-images, because neither the lensing source nor the

background source is sufficiently smooth and axisymmetric to produce a circle. A ring similar to the ORCs could in principle be produced by a lensing cluster of mass $2 \times 10^{15} M_{\odot}$ at a redshift of 1, but (a) there is no sign of a visible cluster within the rings, and (b) it is unlikely that such a lens would be sufficiently symmetric, and perfectly aligned with the background source, to produce the observed circular symmetry.

Ring around Wolf-Rayet star Wolf-Rayet (WR) stars can eject bubbles of material that appear at both radio and optical wavelengths as a ring of emission [38]. About 220 WR stars are known in our Galaxy, although it is estimated that there could be as many as 2000. However, the radio emission associated with WR stars is typically of size a few arcsec or less[39] and they generally have a flatter spectral index than the ORCs[40]. We therefore consider WR stars to be an unlikely cause of the ORCs.

Cluster halo Clusters of galaxies often show diffuse radio halos about an arcmin in diameter [41,42]. However, their morphology is typically irregular, and punctuated by radio emission from their constituent galaxies, and sometimes with a a diffuse relic towards the edge. Radio halo brightness profiles typically peak at the centre and decrease radially without any ring-like structures. They are often observed as patchy, but none, to the best of our knowledge, shows the circularly symmetric edge-brightening seen in the ORCs. Furthermore, cluster halo emission is generally accompanied by a cluster of galaxies and no cluster of galaxies is seen within the ORCs, nor listed in any of the cluster catalogues covering this area (listed by Manojlović et al., 2020, in preparation).

We therefore consider it unlikely that the ORCs are cluster halos. The possibility that ORCs are related instead to radio "relics" seen at the peripheries of merging clusters is discussed in Section 3.

Galactic Wind Termination Shock The winds from star-forming galaxies create a bubble surrounded by a termination shock. For a Milky Way-like galaxy forming $\sim$few $M_{\odot}$/year in an isotropic environment, a roughly spherical galactic wind termination shock at a distance of $\sim$ (few - 10) $\times$ 10 kpc is predicted [43,44]; to reproduce the observed $\sim$1 arcmin angular diameter scale of an ORC, a galaxy with a termination shock at 30 kpc would then need to be located at an angular diameter distance of ~ 100 Mpc or $z \sim 0.02$.

This shock at velocity v will accelerate cosmic ray electrons to an energy limited by inverse Compton cooling of

$$E_{\rm e,max} \sim 10^{13}\ {\rm eV} \left(\frac{B}{0.1\ \mu{\rm G}}\right)^{-1/2} \left(\frac{v}{500\ {\rm km/s}}\right)$$

where we have normalised v to a conservatively small characteristic flow speed and a 0.1 μG field

[45]. This implies that the termination shock associated with a star-forming galaxy should be easily capable of accelerating CR electrons to the $\sim$ few $\times$ 10 GeV energies at which they would produce synchrotron radiation at $\sim$1 GHz.

The energetics of this scenario are also reasonable: assuming that non-thermal electrons account for 1% of the mechanical power dissipated at the putative shock, a mJy source located at $z \sim 0.02$ requires a shock dissipating $\sim 10^{36-37}$ erg/s which can be easily energised by a host with a star formation rate of a few solar masses per year.

While this is a theoretical possibility, such a shock has not yet been observed elsewhere.

4 Conclusion

We have discovered, to the best of our knowledge, a new class of radio-astronomical object, consisting of a circular disc, which in some cases is limb-brightened, and sometimes contains a galaxy at its centre. None of the known types of radio object seems able to explain it. For example, if the ORCs are SNRs, which they strongly resemble, then this implies a population of SNRs in the Galaxy some 50 times larger than the currently accepted figure, or else a new class of SNR which has not previously been reported.

We therefore consider it likely that the ORCs represent a new type of object found in radio-astronomy images. The edge-brightening in some ORCs suggests that this circular image may represent a spherical object, which in turn suggests a spherical wave from some transient event. Several such classes of transient events, capable of producing a spherical shock wave, have recently been discovered, such as fast radio bursts [46], gamma-ray bursts[47], and neutron star mergers[48]. However, because of the large angular size of the ORCs, any such transients would have taken place in the distant past.

It is also possible that the ORCs represent a new category of a known phenomenon, such as the jets of a radio galaxy or blazar when seen end-on, down the "barrel" of the jet. Alternatively, they may represent some remnant of a previous outflow froma. radio galaxy. However, no existing observations of this phenomenon closely resemble the ORCs in features such as the edge-brightening or the absence of a visual blazar or radio galaxy at the centre.

We also acknowledge the possibility that the ORCs may represent more than one phenomenon, and that they have been discovered simultaneously because they match the spatial frequency characteristics of the ASKAP observations, which occupy a part of the observational parameter space which has hitherto been poorly studied.

Further work is continuing to investigate the nature of these objects.

Acknowledgements

We thank Heinz Andernach, Paul Nulsen, Tom Jones, Chris Nolting and many EMU members for valuable comments on an early draft of this paper. Partial support for LR comes from U.S. National Science Foundation grant AST17-14205 to the University of Minnesota. SWD acknowledges an Australian Government Research Training Program scholarship administered through Curtin University. The Australian SKA Pathfinder is part of the Australia Telescope National Facility which is managed by CSIRO. Operation of ASKAP is funded by the Australian Government with support from the National Collaborative Research Infrastructure Strategy. ASKAP uses the resources of the Pawsey Supercomputing Centre. Establishment of ASKAP, the Murchison Radio-astronomy Observatory and the Pawsey Supercomputing Centre are initiatives of the Australian Government, with support from the Government of Western Australia and the Science and Industry Endowment Fund. We acknowledge the Wajarri Yamatji people as the traditional owners of the Observatory site.

References

1. Norris, R. P., Marvil, J., O'Brien, A. & et al. EMU: The Pilot Survey. *Publ. Astron. Soc. Aus.* in preparation (2019).

2. Norris, R. P. *et al.* EMU: Evolutionary Map of the Universe. *Publ. Astron. Soc. Aus.* **28**, 215–248 (2011). 1106.3219.

3. Johnston, S. *et al.* Science with the Australian Square Kilometre Array Pathfinder. *Publ. Astron. Soc. Aus.* **24**, 174–188 (2007). 0711.2103.

4. Johnston, S. *et al.* Science with ASKAP. The Australian square-kilometre-array pathfinder. *Experimental Astronomy* **22**, 151–273 (2008). 0810.5187.

5. McConnell, D. *et al.* The Australian Square Kilometre Array Pathfinder: Performance of the Boolardy Engineering Test Array. *Publ. Astron. Soc. Aus.* **33**, e042 (2016). 1608.00750.

6. Ananthakrishnan, S. & Pramesh Rao, A. The Indian Giant Metrewave Radio Telescope (invited). In *2001 Asia-Pacific Radio Science Conference AP-RASC '01*, 237 (2001).

7. Abbott, T. M. C. *et al.* The Dark Energy Survey: Data Release 1. *Astrophys. J. Supp.* **239**, 18 (2018). 1801.03181.

8. Wright, E. L. *et al.* The Wide-field Infrared Survey Explorer (WISE): Mission Description and Initial On-orbit Performance. *Astron. J.* **140**, 1868–1881 (2010). 1008.0031.

9. Aguado, D. S. *et al.* The Fifteenth Data Release of the Sloan Digital Sky Surveys: First Release of MaNGA-derived Quantities, Data Visualization Tools, and Stellar Library. *Astrophys. J. Supp.* **240**, 23 (2019). 1812.02759.

10. Morrissey, P. *et al.* The Calibration and Data Products of GALEX. *Astrophys. J. Supp.* **173**, 682–697 (2007).

11. Venturi, T. *et al.* The two-component giant radio halo in the galaxy cluster Abell 2142. *Astron. Astrophys.* **603**, A125 (2017). 1703.06802.

12. Intema, H. T., Jagannathan, P., Mooley, K. P. & Frail, D. A. The GMRT 150 MHz all-sky radio survey. First alternative data release TGSS ADR1. *Astron. Astrophys.* **598**, A78 (2017). 1603.04368.

13. Condon, J. J. *et al.* The NRAO VLA Sky Survey. *Astron. J.* **115**, 1693–1716 (1998).

14. Bilicki, M. *et al.* WISE SuperCOSMOS Photometric Redshift Catalog: 20 Million Galaxies over 3/pi Steradians. *Ap J Suppl.* **225**, 5 (2016). 1607.01182.

15. Anderson, L. D. *et al.* Galactic supernova remnant candidates discovered by THOR. *Astron. Astrophys.* **605**, A58 (2017). 1705.10927.

16. Bozzetto, L. M. *et al.* Statistical Analysis of Supernova Remnants in the Large Magellanic Cloud. *Astrophys. J. Supp.* **230**, 2 (2017). 1703.02676.

17. Green, D. A. A revised catalogue of 294 Galactic supernova remnants. *Journal of Astrophysics and Astronomy* **40**, 36 (2019). 1907.02638.

18. Joseph, T. D. *et al.* The ASKAP EMU Early Science Project: radio continuum survey of the Small Magellanic Cloud. *Mon. Not. R. Astron. Soc.* **490**, 1202–1219 (2019). 1909.10425.

19. Maggi, P. *et al.* The supernova remnant population of the Small Magellanic Cloud. *Astron. Astrophys.* **631**, A127 (2019). 1908.11234.

20. Meixner, M. *et al.* Mid-IR and radio images of IC 418: dust in a young planetary nebula. *Astron. Astrophys.* **313**, 234–242 (1996).

21. Bojičić, I. S., Parker, Q. A., Filipović, M. D. & Frew, D. J. Radio-continuum detections of Galactic Planetary Nebulae - I. MASH PNe detected in large-scale radio surveys. *Mon. Not. R. Astron. Soc.* **412**, 223–245 (2011). 1010.4479.

22. Wang, Y. *et al.* Radio continuum emission in the northern Galactic plane: Sources and spectral indices from the THOR survey. *Astron. Astrophys.* **619**, A124 (2018). 1808.05990.

23. Pottasch, S. R. *Planetary nebulae. A study of late stages of stellar evolution*, vol. 107 (1984).

24. Parker, Q. A., Bojičić, I. & Frew, D. J. Exploiting the HASH Planetary Nebula Research Platform. In Liu, X., Stanghellini, L. & Karakas, A. (eds.) *Planetary Nebulae: Multi-Wavelength Probes of Stellar and Galactic Evolution*, vol. 323 of *IAU Symposium*, 36–39 (2017). 1612.00167.

25. Higdon, J. L. Wheels of Fire. II. Neutral Hydrogen in the Cartwheel Ring Galaxy. *Astrophys. J.* **467**, 241 (1996).

26. Pogge, R. W. & Eskridge, P. B. Star Formation in the Disks of H I-Rich SO Galaxies. *Astron. J.* **106**, 1405 (1993).

27. Forbes, D. A., Norris, R. P., Williger, G. M. & Smith, R. C. A Nuclear Starburst Ring in the Spiral Galaxy NGC 7552. *Astron. J.* **107**, 984 (1994).

28. Ulvestad, J. S., Johnston, K. J. & Weiler, K. W. The arc second radio structure of 12 BL Lacertae objects. *Astrophys. J.* **266**, 18–27 (1983).

29. Churazov, E., Brüggen, M., Kaiser, C. R., Böhringer, H. & Forman, W. Evolution of Buoyant Bubbles in M87. *Astrophys. J.* **554**, 261–273 (2001). astro-ph/0008215.

30. Randall, S. W. *et al.* Radio and Deep Chandra Observations of the Disturbed Cool Core Cluster Abell 133. *Astrophys. J.* **722**, 825–846 (2010). 1008.2921.

31. Kang, H. Re-Acceleration of Fossil Electrons by Shocks Encountering Hot Bubbles in the Outskirts of Galaxy Clusters. *Journal of Korean Astronomical Society* **51**, 185–195 (2018). 1812.05773.

32. Kale, R., Dwarakanath, K. S., Bagchi, J. & Paul, S. Spectral and polarization study of the double relics in Abell 3376 using the Giant Metrewave Radio Telescope and the Very Large Array. *Mon. Not. R. Astron. Soc.* **426**, 1204–1211 (2012). 1206.3389.

33. Nolting, C., Jones, T. W., O'Neill, B. J. & Mendygral, P. J. Interactions between Radio Galaxies and Cluster Shocks. I. Jet Axes Aligned with Shock Normals. *Astrophys. J.* **876**, 154 (2019). 1904.05943.

34. Nolting, C., Jones, T. W., O'Neill, B. J. & Mendygral, P. J. Simulated Interactions between Radio Galaxies and Cluster Shocks. II. Jet Axes Orthogonal to Shock Normals. *Astrophys. J.* **885**, 80 (2019). 1909.08721.

35. Pfrommer, C. & Jones, T. W. Radio Galaxy NGC 1265 Unveils the Accretion Shock Onto the Perseus Galaxy Cluster. *Astrophys. J.* **730**, 22 (2011). 1004.3540.

36. Jauncey, D. L. *et al.* An unusually strong Einstein ring in the radio source PKS1830-211. *Nature* **352**, 132–134 (1991).

37. Zitrin, A., Broadhurst, T., Rephaeli, Y. & Sadeh, S. The Largest Gravitational Lens: MACS J0717.5+3745 (z = 0.546). *Astrophys. J. Lett.* **707**, L102–L106 (2009). 0907.4232.

38. Cichowolski, S. *et al.* A DRAO and VLA Investigation of the Environment of WR 130. *Astron. J.* **122**, 1938–1953 (2001).

39. Abbott, D. C., Beiging, J. H., Churchwell, E. & Torres, A. V. Radio Emission from Galactic Wolf-Rayet Stars and the Structure of Wolf-Rayet Winds. *Astrophys. J.* **303**, 239 (1986).

40. Dougherty, S. M. & Williams, P. M. Non-thermal emission in Wolf-Rayet stars: are massive companions required? *Mon. Not. R. Astron. Soc.* **319**, 1005–1010 (2000).

41. Feretti, L., Giovannini, G., Govoni, F. & Murgia, M. Clusters of galaxies: observational properties of the diffuse radio emission. *Astron. Astrophys. Rev.* **20**, 54 (2012). 1205.1919.

42. van Weeren, R. J. *et al.* Diffuse Radio Emission from Galaxy Clusters. *Space Sci. Rev.* **215**, 16 (2019). 1901.04496.

43. Jokipii, J. R. & Morfill, G. Ultra–High Energy Cosmic Rays in a Galactic Wind and Its Termination Shock. *Astrophys. J.* **312**, 170 (1987).

44. Völk, H. J. & Zirakashvili, V. N. Cosmic ray acceleration by spiral shocks in the galactic wind. *Astron. Astrophys.* **417**, 807–817 (2004). astro-ph/0401368.

45. Crocker, R. M., Bicknell, G. V., Taylor, A. M. & Carretti, E. A Unified Model of the Fermi Bubbles, Microwave Haze, and Polarized Radio Lobes: Reverse Shocks in the Galactic Center's Giant Outflows. *Astrophys. J.* **808**, 107 (2015). 1412.7510.

46. Bannister, K. W. *et al.* A single fast radio burst localized to a massive galaxy at cosmological distance. *Science* **365**, 565–570 (2019). 1906.11476.

47. Ayal, S. & Piran, T. Remnants from Gamma-Ray Bursts. *Astrophys. J.* **555**, 23–30 (2001). astro-ph/0011158.

48. Hotokezaka, K. & Piran, T. Mass ejection from neutron star mergers: different components and expected radio signals. *Mon. Not. R. Astron. Soc.* **450**, 1430–1440 (2015). 1501.01986.

49. Condon, J. J. *et al.* The NRAO VLA Sky Survey. *Astron. J.* **115**, 1693–1716 (1998).

50. Gaia Collaboration *et al.* Gaia Data Release 2. Summary of the contents and survey properties. *Astron. Astrophys.* **616**, A1 (2018). 1804.09365.

SUPPLEMENTARY INFORMATION

1 Data availability.

All EMU-PS data (tables and images, and uv data) are available from CASDA on `http://hdl.handle.net/102.100.100/164555?index=1` or from `https://data.csiro.au/dap/public/casda/casdaSearch.zul` under project code AS101. A zoomable image of the EMU-PS survey is available on `http://emu-survey.org`. A listing of observations is on `https://apps.atnf.csiro.au/OMP/index.jsp`.

2 ASKAP Observations

ASKAP consists of 36×12-m antennas, each of which is equipped with a chequerboard Phased Array Feed (PAF), giving a field of view of about 30 square degrees of the sky, resulting in a high survey speed. We used a 36 PAF beams, with the beam centres separated by 0.9 degrees, arranged in the "Closepack36" configuration[1]. A full description of ASKAP may be found in Hotan et al. (2020; in preparation).

The EMU Pilot Survey[1] (hereafter EMU-PS), the source of the discoveries described here, consists of ten observations, each lasting 10–12 hours, in the period 15 July to 24 November 2019. Between 32 and 36 ASKAP antennas were used in each observation, always including the outer four, with baselines up to 6.4 km, with the remaining antennas within a region of 2.3 km diameter. Specifications of the observations are given in Table 1.

We processed the data using the ASKAPsoft pipeline[1,2], including w-projection multifrequency synthesis imaging, multiscale clean, and self-calibration.

3 ATCA Observations

We observed ORC 1 and ORCs 2–3 (Project code C3350) with the Australia Telescope Compact Array (ATCA) on 9–10 April 2020, at 1.1–3.1 GHz (weighted central frequency after the removal of radio frequency interference = 2121 MHz), over a period of 2×12 hours using the 6A configuration. The data were processed using miriad, using the standard ATCA multi-frequency synthesis process, and cleaned with a robustness of +0.5. The observations were affected by radio frequency interference, resulting in a relatively high rms of $\sim$ 10–15 μJy/beam, with a synthesised beamsize of 5.0×4.3 arcsec.

Table 1: EMU Pilot Survey Specifications

Area of survey	270 deg^2
Field centre	21h, –55 degr
Synthesised beamwidth	$13'' \times 11''$ FWHM
Frequency range	800 – 1088 MHz
Observing configuration	closepack36, pitch 0.9°
	no interleave
Weighting	Robust = 0
RMS sensitivity	25 – 35 μJy/beam
Total integration time	100 hours
Number of sources detected	$\sim$250,000

4 GMRT Observations

ORC-4 was found in archival 325 MHz GMRT data taken on the cluster source project (ID 23 017)[3] on the cluster Abell 2142. The data were reprocessed with the SPAM pipeline[4] yielding a sensitivity of 47 μJy/beam at the field center, and a resolution of 9.4 $\times$ 7.9 arcsec. At the location of the ring the sensitivity is 66 μJy/beam, mainly due to primary beam attenuation.

5 MWA Observations

The observations with the Murchison Widefield Array[5] in its 'Phase II' extended configuration (hereafter MWA-2[6]) were taken as part of project G0045 which aims to image diffuse, non-thermal radio emission in galaxy clusters across five frequency bands of $\Delta\nu = 30$ MHz centered on 88, 118, 154, 185, and 216 MHz. As these observations have a large field of view, ORC1 and ORC2 fall within the primary beam main lobe half power point in one of the observed fields: 'FIELD4'. MWA observations of this form are taken in a 2-min snapshot mode due to a fixed primary beam. All data undergo radio frequency interference flagging using `AOFlagger`[7]. To increase integration time on a source, large numbers of 2-min snapshots are independently calibrated with the full-Jones `Mitchcal` algorithm[8], independently imaged, and finally stacked in the image plane as a linear mosaic.

MWA-2 data reduction for this work follows the process described in detail by Duchesne et al. (submitted), using a purpose-written MWA-2 pipeline (`piip` [2]).

6 Radio properties

To measure flux densities, we used the measure_source.py tool [3], in which a polygon is drawn around the source[9] The resulting flux densities are shown in Table 2.

Spectral indices were derived by weighted least-squares fitting to the flux densities listed in the Tables, assuming a power-law spectral energy distribution. The uncertainty on the spectral index was estimated using the leastsq algorithm in scipy.optimize[4].

[2] `https://gitlab.com/Sunmish/piip`

[3] `https://github.com/nhurleywalker/polygon-flux`

[4] `https://docs.scipy.org/doc/scipy/reference/optimize.html`

7 Optical/IR properties

The redshifts listed in Table 4 are taken from the Dark Energy Survey photometric redshift survey[10], which are most reliable in the redshift range 0.5–1, and so we do not regard these redshifts as reliable.

Photometry for the galaxies that may be associated with the ORCs were taken from the DES[7], WISE[11], and GALEX[12] surveys and are listed in Tables 4 to 5.

Galaxy classification was estimated using the WISE colours, following the WISE colour-colour diagram[11], and also using the DES and Galex colours in a colour-magnitude diagram[13]. However these classifications are quite uncertain because most of the galaxies do not have a spectroscopic redshift.

References for Supplementary Information

1. Norris, R. P., Marvil, J., O'Brien, A. & et al. EMU: The Pilot Survey. in preparation (2019).

2. Whiting, M., Voronkov, M., Mitchell, D. & ASKAP Team. Early Science Pipelines for ASKAP, vol. 512 of Astronomical Society of the Pacific Conference Series, 431 (2017).

3. Venturi, T. et al. The two-component giant radio halo in the galaxy cluster Abell 2142. A&A 603, A125 (2017). 1703.06802.

4. Intema, H. T., Jagannathan, P., Mooley, K. P. & Frail, D. A. The GMRT 150 MHz all-sky radio survey. First alternative data release TGSS ADR1. A&A 598, A78 (2017). 1603.04368.

5. Tingay S. J., et al., The Murchison Widefield Array: The Square Kilometre Array Precursor at Low Radio Frequencies, PASA, 30 e007 (2013)

6. Wayth, R. B. et al. The Phase II Murchison Widefield Array: Design overview. PASA 35 (2018). 1809.06466.

7. Offringa A. R., et al., The Low-Frequency Environment of the Murchison Widefield Array: Radio-Frequency Interference Analysis and Mitigation, PASA, 32, e008 (2015)

8. Offringa A. R., et al., Parametrizing Epoch of Reionization foregrounds: a deep survey of low-frequency point-source spectra with the Murchison Widefield Array, MNRAS, 458, 1057 (2016)

9. Hurley-Walker, N. et al. Candidate radio supernova remnants observed by the GLEAM survey over $345 < l < 60$ and $180 < l < 240$. PASA, 36, e048 (2019). 1911.08124.

10. Abbott, T. M. C. et al. The Dark Energy Survey: Data Release 1. ApJS, 239, 18 (2018). 1801.03181.

11. Wright, E. L. et al. The Wide-field Infrared Survey Explorer (WISE): Mission Description and Initial On-orbit Performance. AJ 140, 1868–1881 (2010). 1008.0031.

12. Morrissey, P. et al. The Calibration and Data Products of GALEX. ApJS 173, 682–697 (2007).

13. Schawinski, K. et al. The green valley is a red herring: Galaxy Zoo reveals two evolutionary pathways towards quenching of star formation in early- and late-type galaxies. MNRAS, 440, 889–907 (2014). 1402.4814.

Table 1: The new circular objects ("ORCs")

ID	Name	RA (deg) J2000	Dec (deg) J2000	l (deg)	b (deg)	survey
ORC 1	EMU PD J210357.9–620014	315.74292	–62.00444	333.41592	-39.00906	EMU-PS
ORC 2	EMU PD J205842.8–573658	314.67833	–57.61611	339.08813	-39.52277	EMU-PS
ORC 3	EMU PD J205856.0-573655	314.73458	–57.61528	339.08147	-39.55247	EMU-PS
ORC 4	155524.63+272634.7	238.85272	+27.44271	44.35860	49.36566	GMRT

Table 2: Integrated Flux Densities (in mJy) and spectral indices of the radio sources associated with ORCs 1–3. We estimate an uncertainty of 20% on all flux density measurements. Measurements at 88, 118, and 154 MHz are made with MWA. Measurements at 944 MHz are made with ASKAP. Measurements at 2121 MHz are made with ATCA. MWA measurements of ORC 1 include the flux density of source S, and MWA measurements of ORC 2 include the flux density of source C. However, these will have a negligible effect on the fitted spectral indices.

source	88 MHz	118 MHz	154 MHz	944 MHz	2121 MHz	α
ORC 1	105±16.5	69.5±8.6	38±6.0	6.26±1.25	2.29±0.23	–1.17±0.04
ORC 1(S)		.		0.60±0.12	0.15±0.03	–1.71±0.35
ORC 2	28±14.4	25±6.8	14±5.3	6.97±1.39	2.31±0.23	–0.80±0.08
ORC 2(A)				0.46±0.10	0.46±0.05	0.0±0.34
ORC 2(B)				0.76±0.15	0.66±0.07	–0.17±0.22
ORC 2(C)				0.19±0.05	0.07±0.03	–1.23±0.36
ORC 3			<5	1.86±0.37	<1.0	–0.50±0.20

Table 3: Measured Flux Densities (in mJy) of the radio sources associated with ORC 4. 150 MHz data are from TGSS[12], 325 MHz data are from the observations described in the text, and 1400 MHz data are from the NVSS survey[49]. The flux densities for the ring are the total flux densities (including source G) measured in a 2 arcmin diameter aperture, and that for source G is from a fitted Gaussian component.

source	150 MHz	325 MHz	1400 MHz	α
ORC 4	39±10	28±2.8	5.3±0.7	–0.92±0.18
ORC 4(G)		1.43±0.13		

Table 4: Properties of the optical/IR sources near ORCs 1–2

Source Name	ID	ASKAP	GALEX		DES					WISE					Notes
		flux	FUV	NUV	g	r	i	z	Y	W1	W2	W3	W1–W2	z	
		[mJy]	[mag]				[mag]				[mag]				
WISE J210258.15–620014.4	ORC 1 C	< 0.1	—	—	22.04	20.10	19.23	18.79	18.70	15.065	14.984	>12.939	0.081	??	
					0.06	0.01	0.01	0.02	0.04	±0.031	±0.061				
WISE J210257.88–620046.3	ORC 1 S	0.86	23.7	22.3	19.733	18.945	18.550	18.351	18.311	15.472	15.063	11.201	0.409	??	
			±1.2	±0.3	0.005	0.003	0.005	0.008	0.023	±0.034	±0.057	±0.138			
WISE J205851.65–573554.1	ORC 2 A	1.0	25.9	20.9	17.676	17.355	17.263	17.253	17.352	16.038	16.501	>12.716	–0.463	1.37	listed as a star in Gaia DR2[50]
			4.0	0.1	0.001	0.001	0.001	0.002	0.01	±0.050	±0.252				
WISE J205848.80–573612.1	ORC 2 B	1.7	—	—	20.53	19.03	18.52	18.20	18.09	15.138	14.995	>12.431	0.143	0.35	2.5 arcsec extended spiral galaxy
					0.02	0.01	0.01	0.01	0.05	±0.035	±0.071				
WISE J205847.91–573653.8	ORC 2 C	0.2?	—	—	21.38	20.95	20.82	20.72	20.37	15.499	14.930	11.729	0.569		edge-on galaxy
					0.02	0.02	0.02	0.03	0.2	±0.041	±0.066	±0.232			

Table 5: Properties of the optical/IR source at the centre of ORC 4

Source Name	ID	GMRT	GALEX		SDSS					WISE					Notes
		flux	FUV	NUV	u	g	r	i	z	W1	W2	W3	W1–W2	z	
		[mJy]	[mag]				[mag]				[mag]				
WISE J155524.65+272633.7	G	1.15	—	—	22.61	21.18	19.64	19.00	18.40	14.847	15.119	12.341	–0.272	0.385	
SDSS J155524.63+272634.3		?			±0.70	±0.09	±0.03	±0.03	±0.06	±0.057	±0.112	±0.483	±0.126		

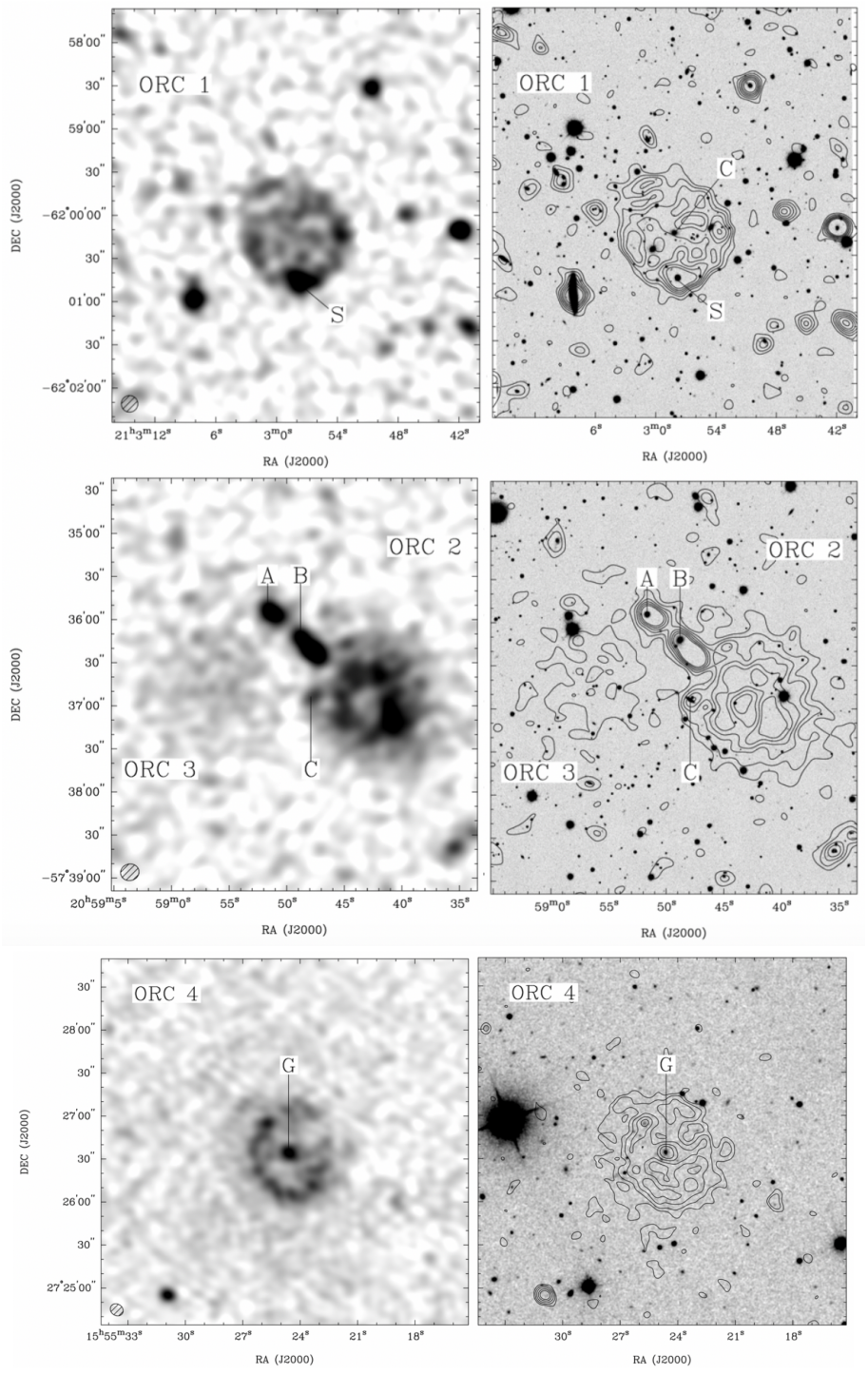

Figure 1: ASKAP radio continuum images at 944 MHz of ORCs 1–3 from the EMU Pilot Survey[1], and at 325 MHz of ORC 4 from GMRT archival data. On the left are greyscale images, with the synthesized beam shown in the bottom left corner, and radio contours overlaid onto DES optical images on the right, as described in the text. The contour levels for ORC 1 and ORC 2 are 45, 90, 135, 180, 225, and 270 μJy beam^{-1}, and contour levels for ORC 4 are 150, 250, 400, 600, and 800 μJy beam^{-1}. Sources of interest are labelled (see Tables 3 & 4).

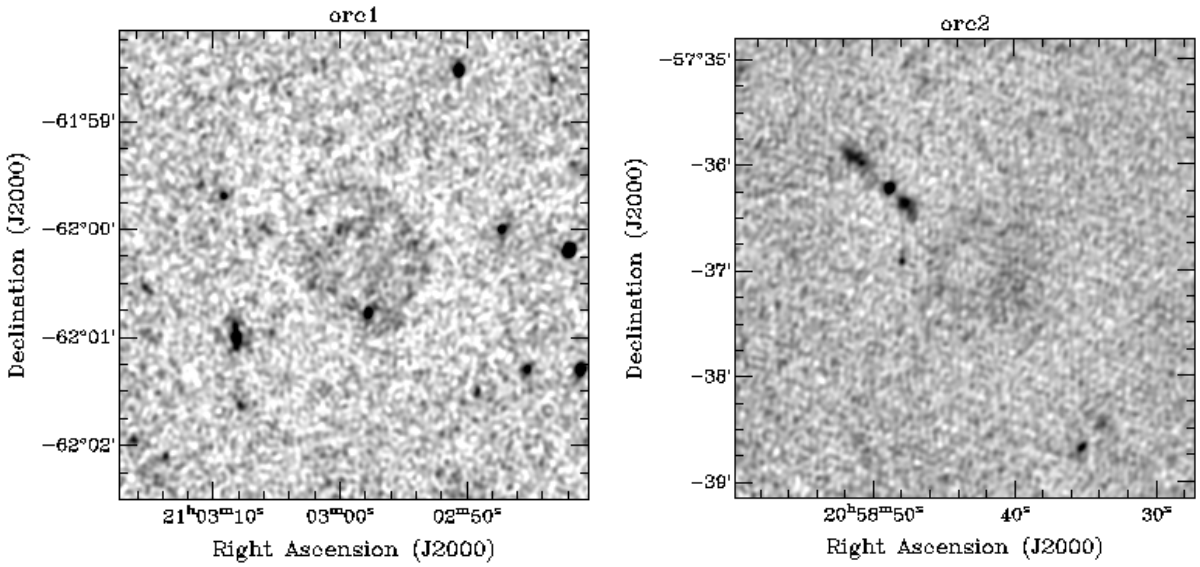

Figure 2: ATCA radio continuum images of ORCs 1–3 at a frequency of 2.1 GHz. The image rms is about 12 μJy/beam in both images. ORCs 1 and 2 are only faintly visible in these higher-frequency images, because of their steep spectral index and higher resolution, while ORC 3 is below the rms noise level. This image shows that sources A and B in ORC 2 are the two lobes of an FRI radio galaxy.

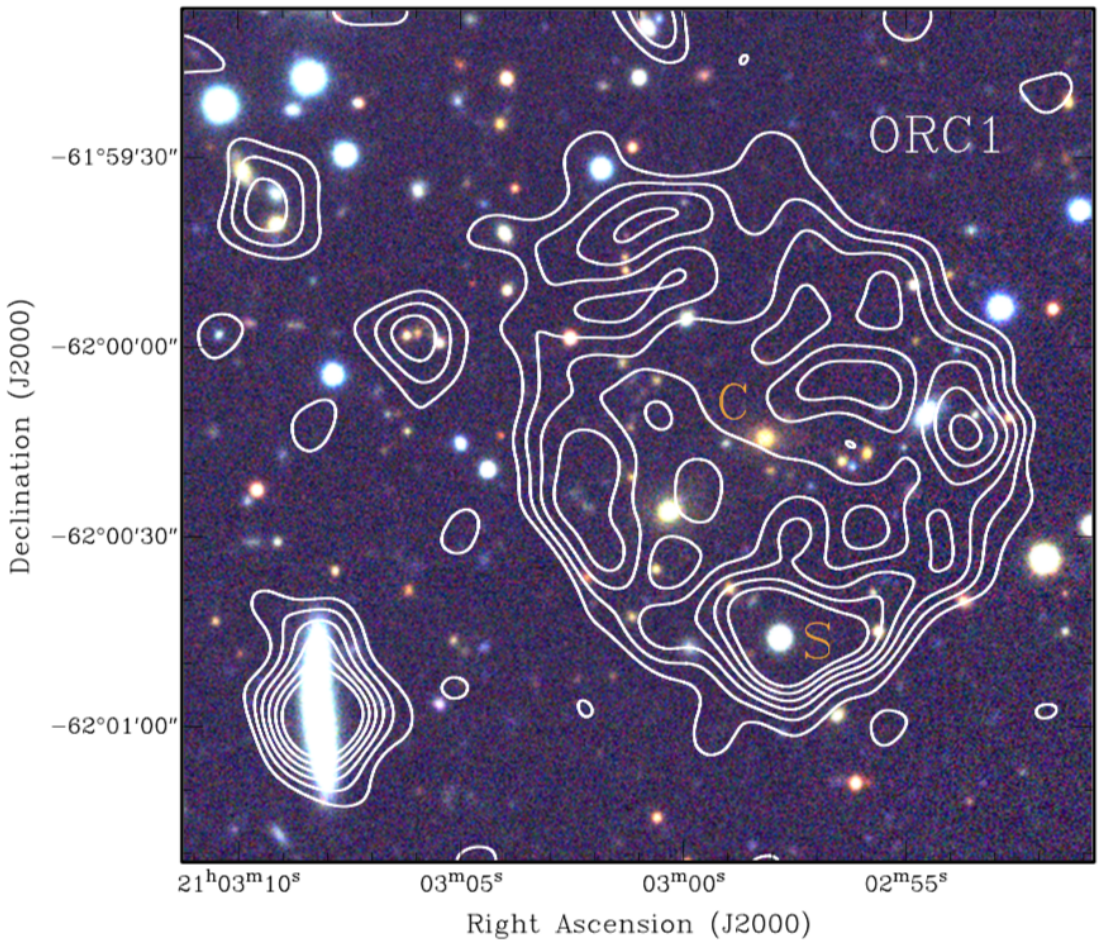

Figure 3: ASKAP radio continuum image of ORC 1 (contours; see Fig. 1) overlaid onto a DES 3-color composite image; DES *gri*-bands are colored blue, green, and red, respectively. We identify two galaxies of interest: "C" lies near the centre of ORC 1 and "S" coincides with the southern radio peak (see Table 3).

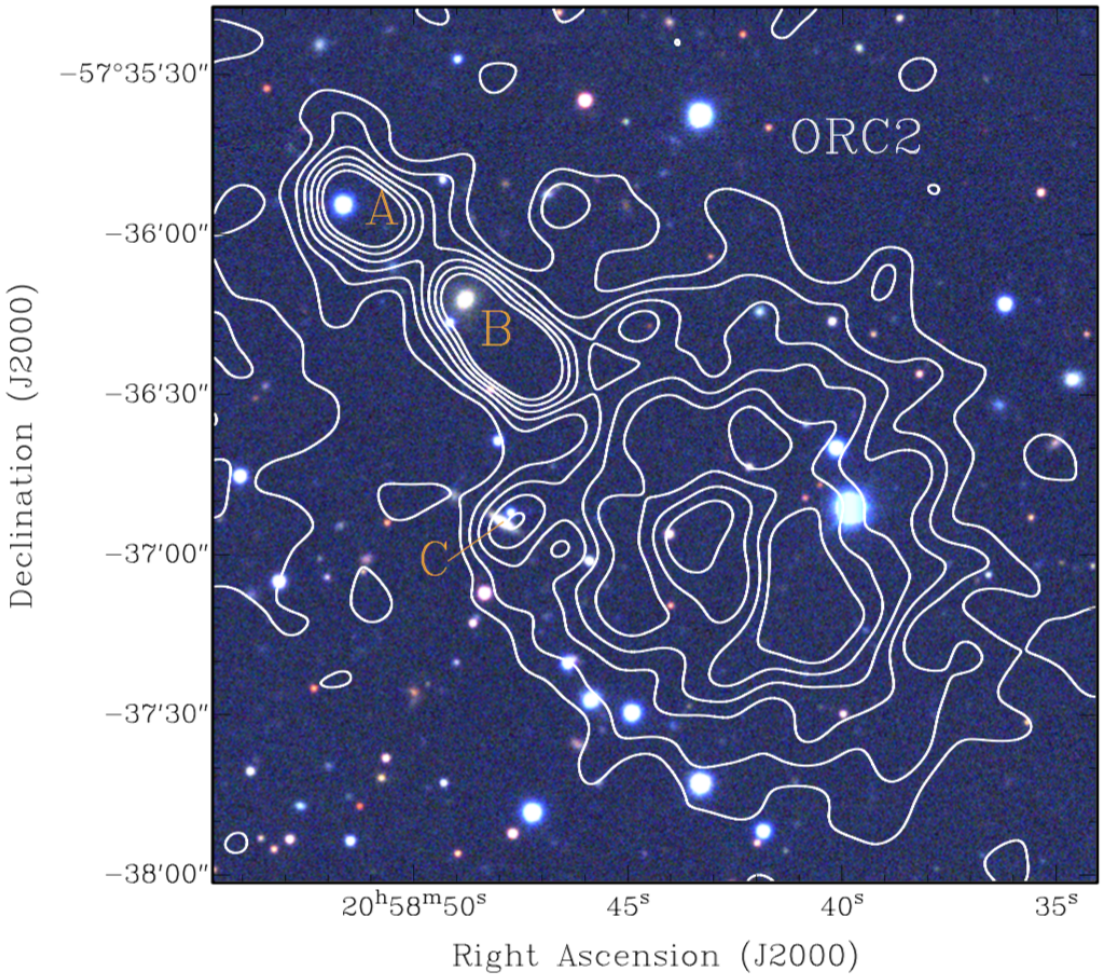

Figure 4: ASKAP radio continuum image of ORC 2 (contours; see Fig. 1) overlaid onto a DES 3-color composite image; DES *gri*-bands are colored blue, green, and red, respectively. We identify three sources of interest, annotated A, B and C (see Table 4).

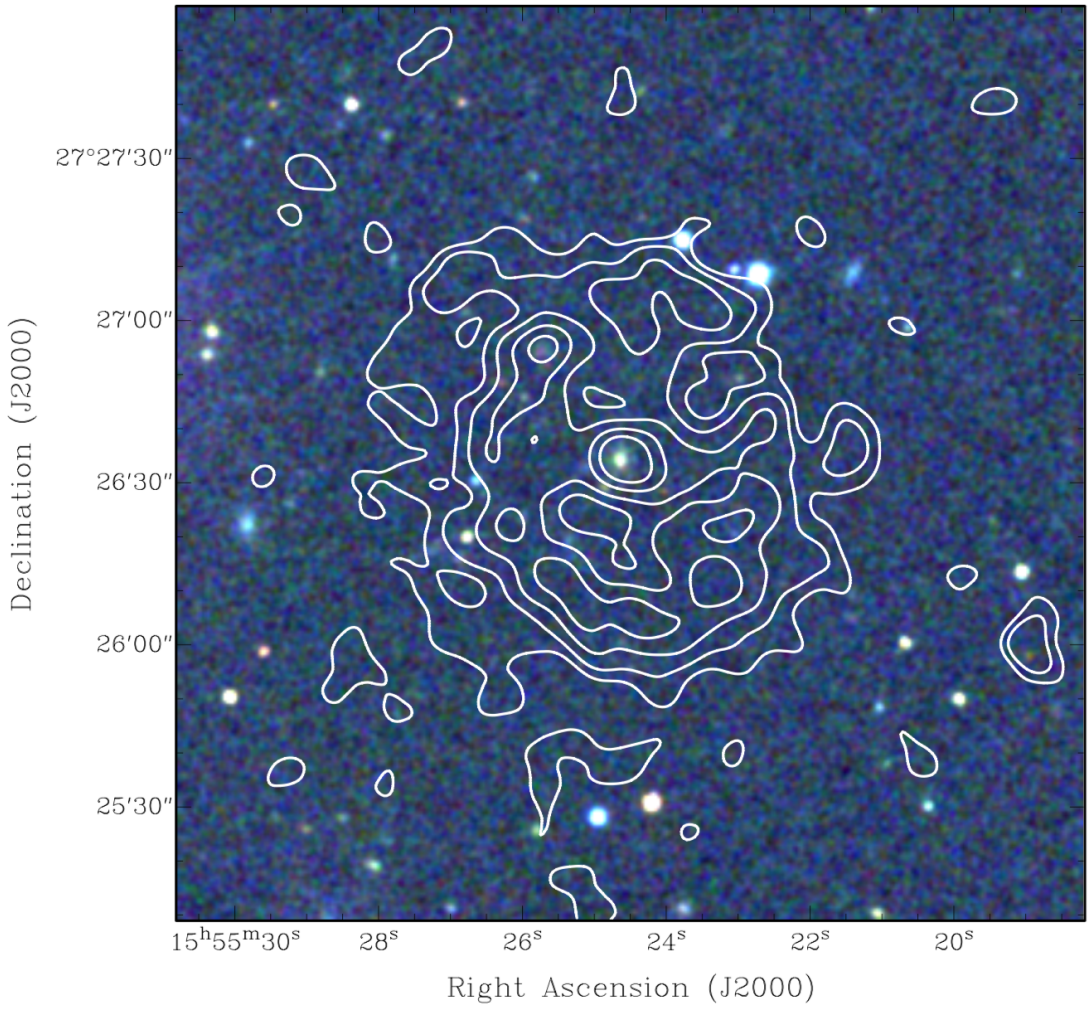

Figure 5: GMRT radio continuum image of ORC 4 (contours; see Fig. 1) overlaid onto a SDSS 3-color composite image; SDSS *gri*-bands are colored blue, green, and red, respectively.

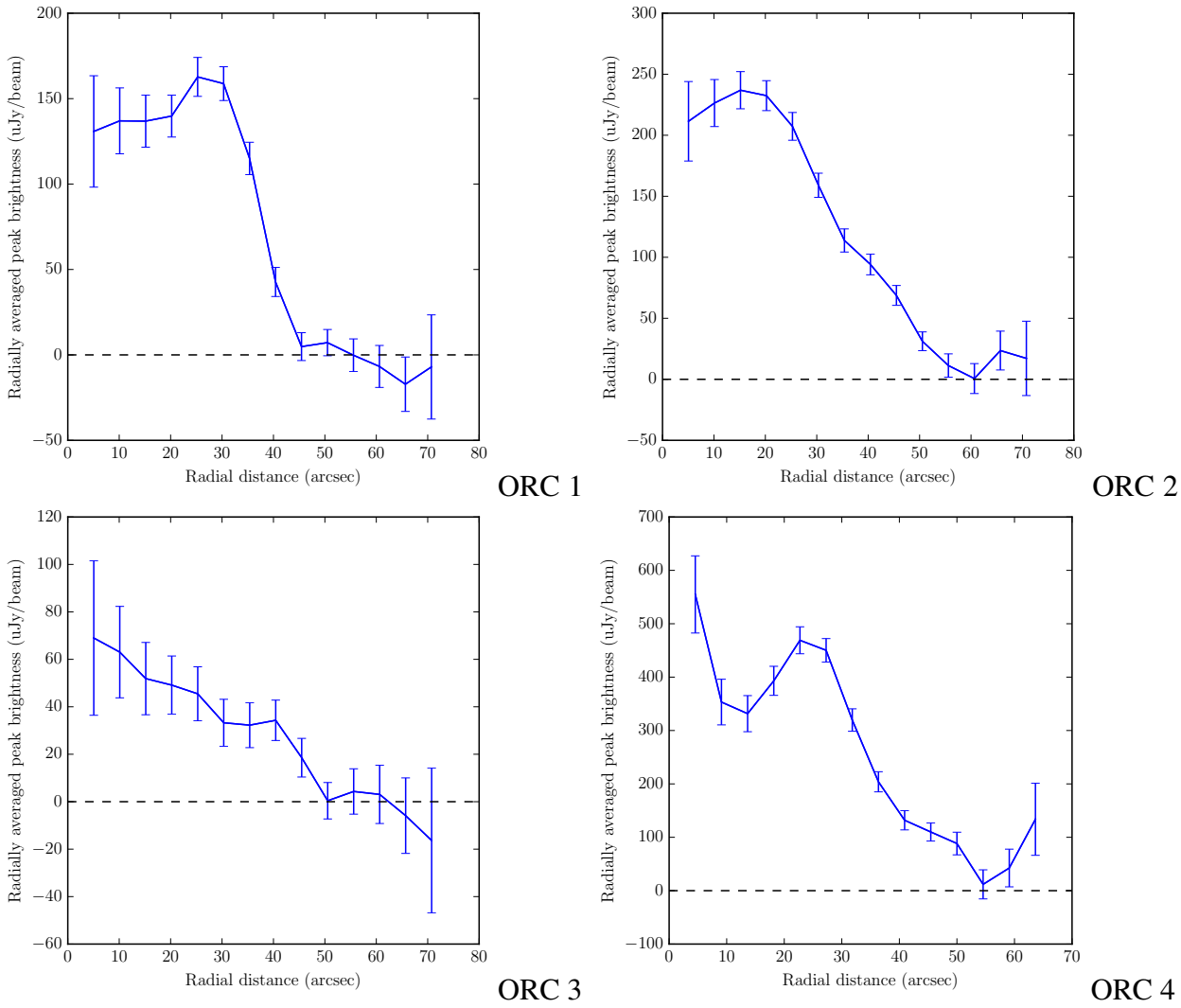

Figure 6: Radial profiles of the diffuse emission of the ORCS, measured from the ASKAP and GMRT data, and integrated radially around the ORC, assuming circular symmetry, after removing compact sources A and B in ORC 2. Error bars are σ / sqrt (number of independent beam volumes), where $\sigma = 25\,\mu$Jy/beamfor the EMU data (ORCS 1, 2, and3), and $60\,\mu$Jy/beamfor the uGMRT data (ORC 4).

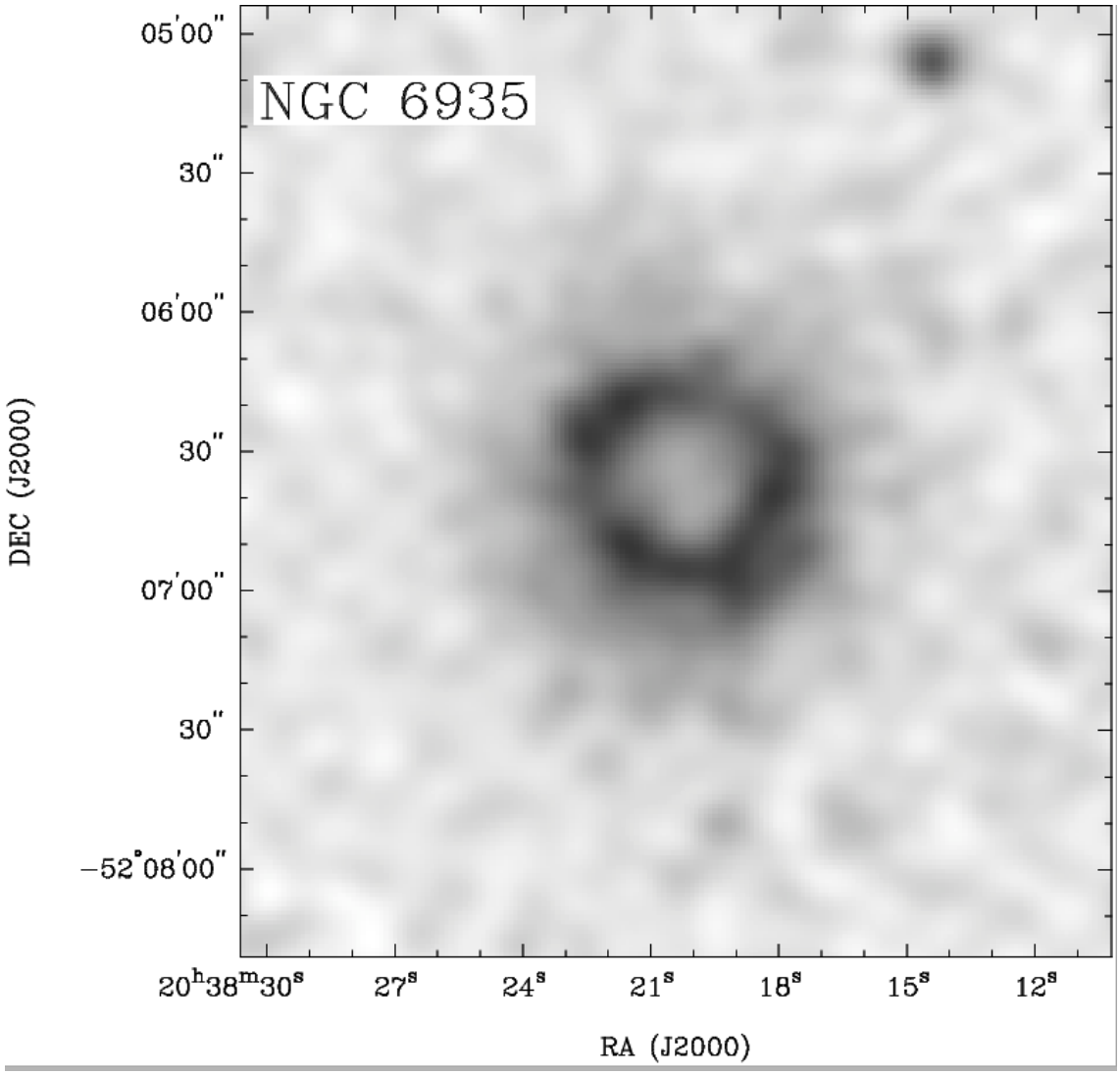

Figure 7: ASKAP 944 MHz radio continuum image of the face-on, star-forming galaxy NGC 6935 (v = 4543 km s^{-1}), as observed in the EMU-PS.

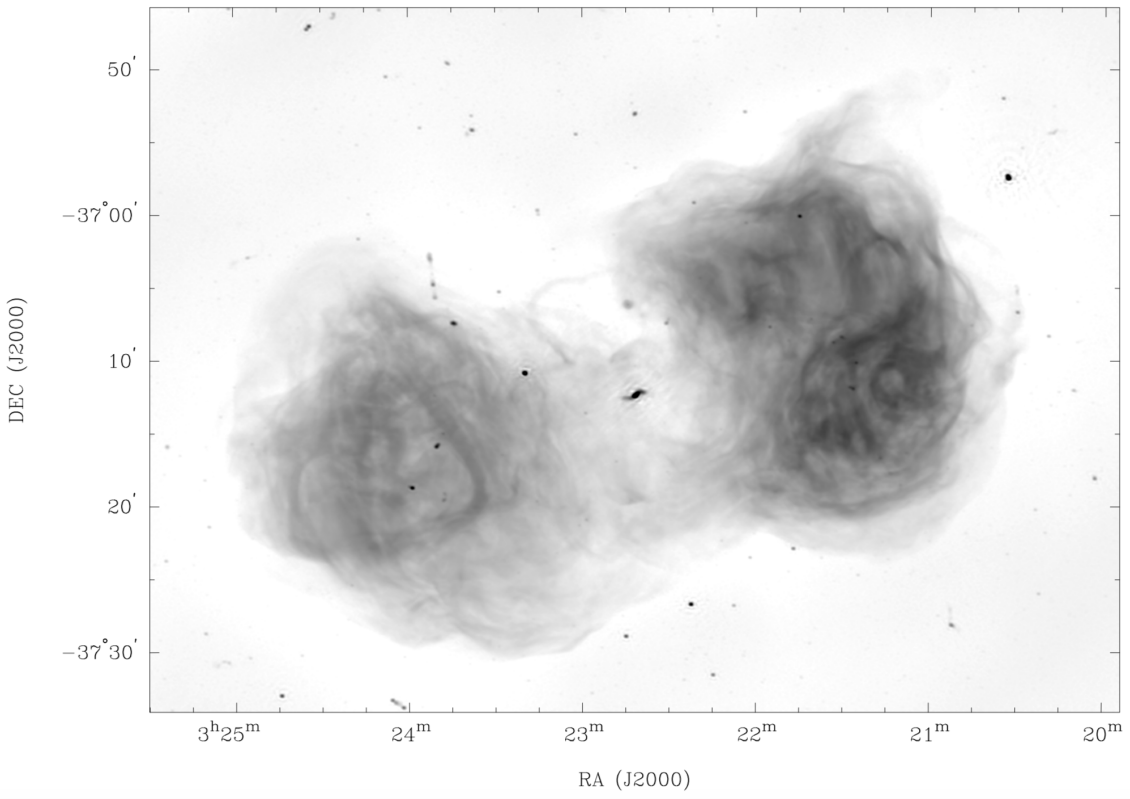

Figure 8: ASKAP 944 MHz radio continuum image of the double-lobe radio galaxy Fornax A, from unpublished ASKAP data.

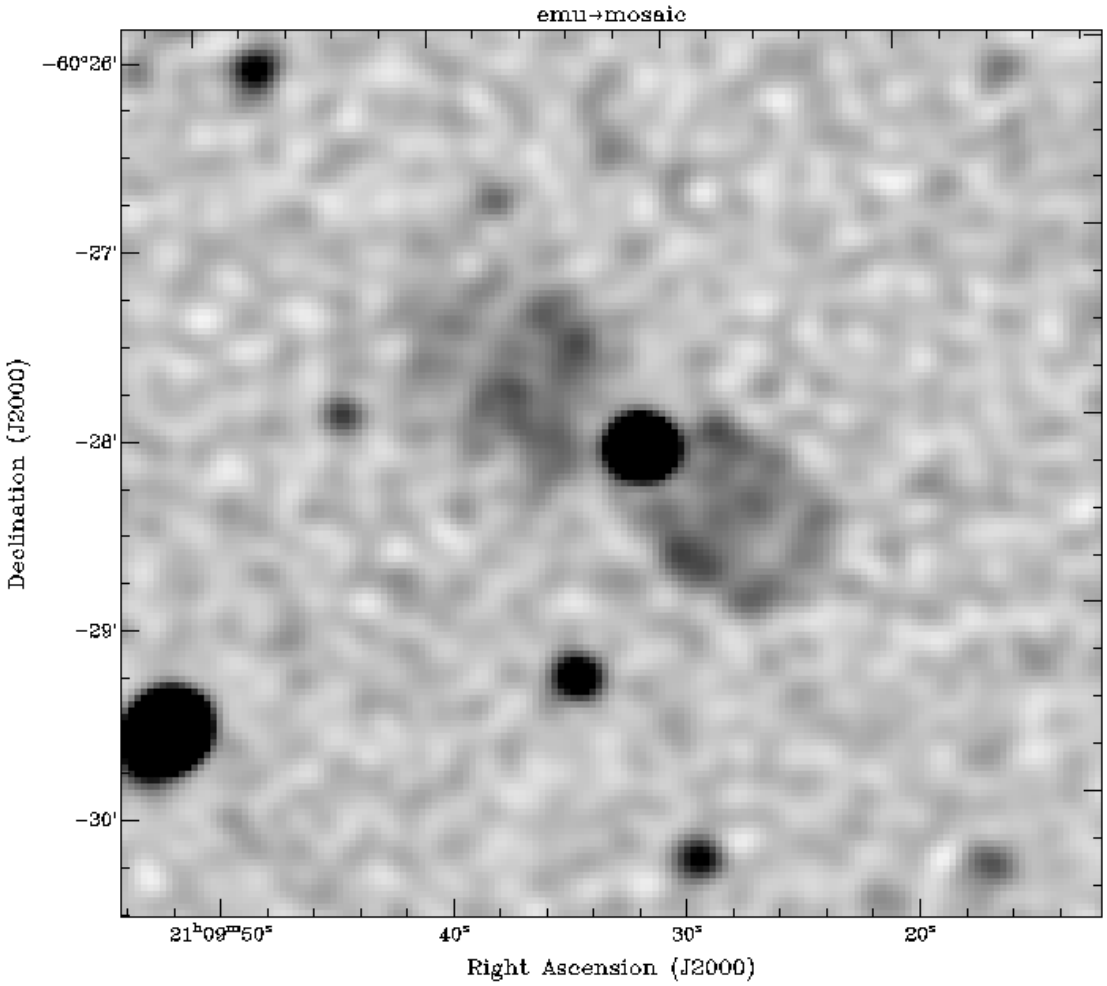

Figure 9: EMU-PS image of the edge-brightened double-lobe radio galaxy EMU PD J2109:31.3-602806

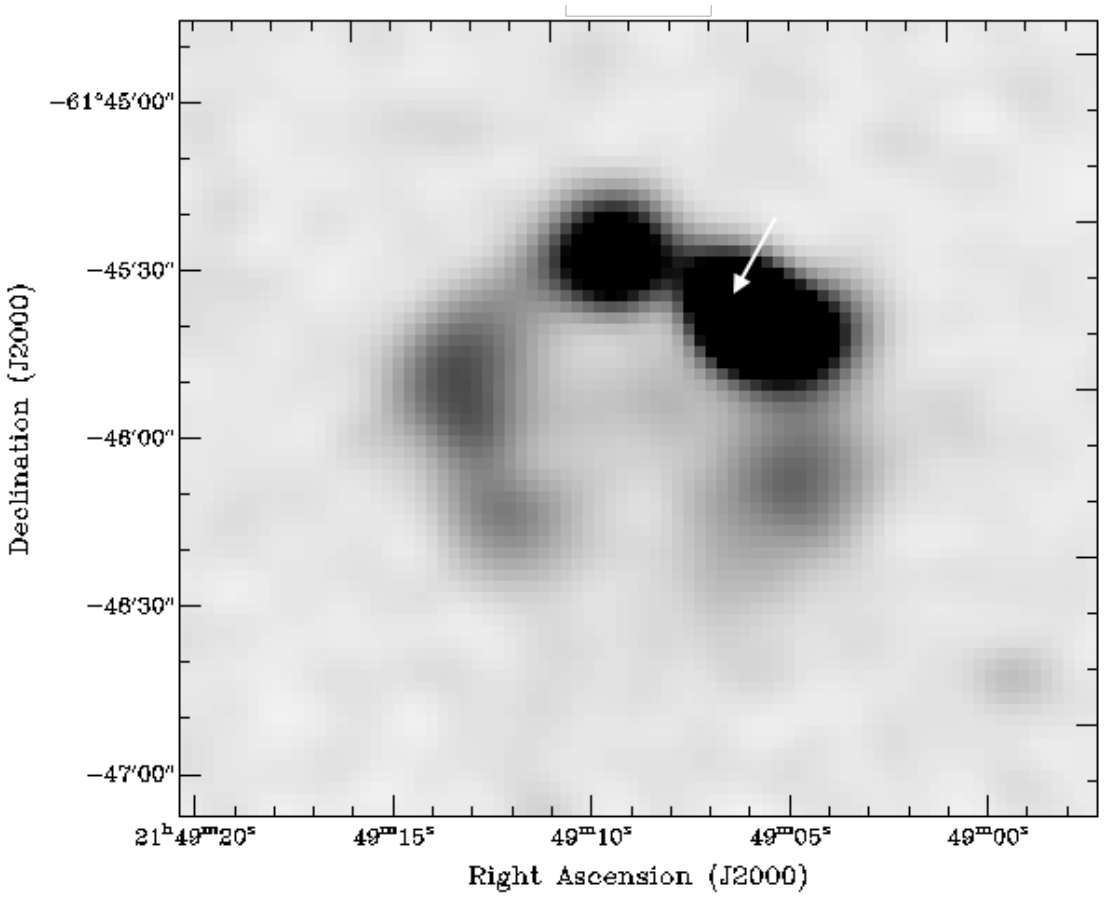

Figure 10: EMU-PS image of the bent-tail radio galaxy EMU PD J214905.4-614542. The position of the host galaxy is indicated by an arrow.